Crystal growth, superconductivity, and charge density wave of pristine and Pd-intercalated 2*H*-TaS_2

Shunli Ni,[1,*,†] Menghu Zhou,[2,*,‡] Zefeng Lin,[2] Binbin Ruan,[2] Zhifeng Li,[1] Zhiwei Zou,[1] Zhenghua Xu,[1] and Zhi-an Ren[2,§]

[1]*School of Mathematics and Physics, University of South China, Hengyang 421001, China*

[2]*Beijing National Laboratory for Condensed Matter Physics, Institute of Physics, Chinese Academy of Science, Beijing 100190, China*

(Received 10 May 2023; revised 13 July 2023; accepted 14 July 2023; published 2 August 2023)

Here, pristine and Pd-intercalated 2*H*-TaS_2 single crystals with (00*l*) orientation were grown by the chemical vapor transport technique. The superconductivity (SC) and charge density wave (CDW) were characterized by magnetic and electrical transport measurements. We find that SC and CDW in the pristine 2*H*-TaS_2 condense respectively at transition temperatures $T_c \sim 0.8$ K and $T_{CDW} \sim 78$ K. The CDW order is completely suppressed, and T_c is greatly enhanced to 4.5 K in 2*H*-$Pd_{0.04}TaS_2$, which concludes a competing relation between the two collective electronic states. The positive Hall coefficient R_H for both samples above 78 K indicates that hole-type carriers dominate the transport properties, and almost the same R_H reveals tiny charge transfer between the intercalant Pd and the host TaS_2. The difference of R_H below 78 K between TaS_2 and $Pd_{0.04}TaS_2$ is attributed to the reconstruction of the Fermi surface by Pd-intercalation-induced collapse of the CDW order. Therefore, the prominently improved T_c in 2*H*-$Pd_{0.04}TaS_2$ is mainly caused by the change of electronic structure due to the suppression of the CDW state rather than charge injection by Pd intercalation.

DOI: 10.1103/PhysRevB.108.075103

I. INTRODUCTION

As a member of the quasi-two-dimensional transition metal dichalcogenides (TMDs), TaS_2 has drawn continuous research attention recently due to its diverse structural phases and abundant electronic properties [1,2]. 1*T*-TaS_2 hosts a sequence of successive charge-density-wave (CDW) transitions, the Mott phase [3,4] and possible quantum spin-liquid state [5,6]. Ising superconductivity (SC) was observed in monolayer TaS_2 (1*H*-TaS_2) [7], and chiral SC has been reported recently in CDW material 4H_b-TaS_2 which exhibits strong spin fluctuations [8,9]. The subject of this paper 2*H*-TaS_2 undergoes a CDW transition at ~78 K and a superconducting transition at ~0.8 K, and chiral charge order was revealed by scanning tunneling spectroscopy [10]. Therefore, TaS_2 is thought to be an important material for probing the relationship of various electronic orders in correlated electron systems. SC and CDW are two competing many-body collective electronic states frequently occurring in quasi-two-dimensional TMDs. The origin of both quantum states is driven by Fermi surface instability and electron-phonon coupling (EPC). The two electronic phenomena can be modulated extensively via various ways, such as high pressure [3,11–15], ionic-liquid gating [16–20], and chemical doping [21–29]. Another aspect is that the van der Waals structure of TaS_2 makes it an excellent platform to explore electronic phenomena [9,30,31] and build quantum devices [32,33].

Several mechanisms behind the formation of CDW in 2*H*-TaS_2 were proposed, including Fermi surface nesting [34], saddle points near the Fermi surface [35], and momentum-dependent EPC [36–39]. The SC and CDW orders, and the interplay between them, have been widely investigated by intercalation of alkali metals, transition metals, and organic molecules into the van der Waals gap of 2*H*-TaS_2 in the past decades [40–45]. The doping dependence of electronic phase diagrams were obtained for the intercalated 2*H*-TaS_2 system [42–45]. Upon intercalation, T_{CDW} decreases, but T_c increases, yielding strong evidence for the competition between these two orders. Recently, we have successfully synthesized a series of 2*H*-Pd_xTaS_2 ($0.01 \leqslant x \leqslant 0.08$) polycrystalline samples. The CDW state was inhibited progressively upon Pd intercalating, and the maximum T_c of 4.2 K was observed at $x = 0.04$ [46]. Tunable SC and CDW in this system make it a superior platform for experimentally studying the evolution of electronic properties at the normal and superconducting states with doping. However, there is still a lack of 2*H*-Pd_xTaS_2 single crystals, which prevents in-depth investigation into the effect of nonmagnetic dopant Pd intercalation on SC and CDW in 2*H*-TaS_2. Although a wide variety of two-dimensional atomically thin TMD materials could be prepared by molten-salt-assisted chemical vapor deposition [47], it is very difficult to acquire pure and intercalated 2*H*-TaS_2 bulk single crystals with high quality due to the stacking faults that often emerge along the *c* axis in TMDs and due to the intergrowth with 3*R* and 4*H* polytypes because of small formation-energy differences [28,30,41,42,48,49].

In this paper, we present a study on the high-quality pristine and Pd-intercalated 2*H*-TaS_2 single crystals by transport and magnetic measurements to further shed light on the variation of electronic properties and the relationship between SC and

*These authors contributed equally to this work.
†nishunli0415@163.com
‡zhoumenghu@iphy.ac.cn
§renzhian@iphy.ac.cn

CDW. The CDW transition at 78 K for $2H$-TaS_2 completely vanishes in $2H$-$Pd_{0.04}TaS_2$, while T_c is boosted from 0.8 K in $2H$-TaS_2 to 4.5 K in $Pd_{0.04}TaS_2$, which is the highest T_c in the fifth- and sixth-row-metal-intercalated $2H$-TaS_2 hitherto. The Hall effect measurements indicate that the transport properties are governed by hole-type carriers, and the charge transfer between Pd and TaS_2 layers is diminutive. The difference in Hall coefficient R_H below 78 K between the two samples implies the reconstruction of the Fermi surface after destroying the CDW condensation. In this paper, we suggest that the markedly improved T_c is mainly caused by the development of electronic structure due to the suppression of the CDW state rather than carrier injection by Pd intercalation, which confirms that SC and CDW orders are competitive in this system.

II. EXPERIMENT

The pristine and Pd-intercalated $2H$-TaS_2 single crystals studied here were grown using the chemical vapor transport (CVT) technique with iodine as a transport agent. High-purity Pd (Alfa Aesar, 99.998%), Ta (Alfa Aesar, 99.999%), and S (Alfa Aesar, 99.999%) with molar ratio x:1:2 ($x = 0, 0.04$) were thoroughly mixed with iodine (5 mg/cm^3) and sealed in an evacuated quartz tube. The sealed quartz tube was placed in a horizontal two-zone tubular furnace. The source and growth zones were heated to 870 and 750 °C in 24 h, respectively, and kept at this temperature gradient for 15 d and followed by natural cooling to room temperature. Finally, shiny $2H$-Pd_xTaS_2 ($x = 0, 0.04$) single crystals with hexagonal morphology were yielded. The x-ray diffraction (XRD) patterns at room temperature for phase identification were recorded on a PANalytical diffractometer with Cu-$K\alpha$ radiation. The magnetic susceptibility for down to 0.4 and 2 K was measured on a Quantum Design MPMS-3 system equipped with and without an iHe3 insert, respectively. The electrical transport measurements were conducted on a Quantum Design PPMS-16T system. In-plane resistivity ρ_{ab} and Hall resistivity ρ_{xy} were measured using the six-probe method. The Hall resistivity ρ_{xy} was precisely determined by the difference of the transverse resistivity in positive and negative fields, i.e., $\rho_{xy}(\mu_0 H) = [\rho_{xy}(\mu_0 H) - \rho_{xy}(-\mu_0 H)]/2$, to eliminate the longitudinal resistivity contributions resulting from the voltage probe misalignment.

III. RESULTS AND DISCUSSION

Figure 1(b) shows the room temperature XRD patterns of the pristine and Pd-intercalated $2H$-TaS_2 single crystals. Only single-preferred ($00l$) orientation for both single crystals has been observed. Compared with $2H$-TaS_2, the diffraction peaks of $2H$-$Pd_{0.04}TaS_2$ shift consistently to lower angles, which can be seen more obviously in the inset of Fig. 1(b), evincing the enlargement of the c axis after Pd intercalation. The c-axis lattice parameters of $2H$-TaS_2 and $2H$-$Pd_{0.04}TaS_2$ calculated from the ($00l$) peaks are 12.081 and 12.109 Å, respectively, which are consistent with the previously reported values [46,50]. Remarkable c-axis expansion by only 4% Pd doping demonstrates that Pd atoms intercalate into the van der Waals gaps between the neighboring TaS_2-trigonal prismatic

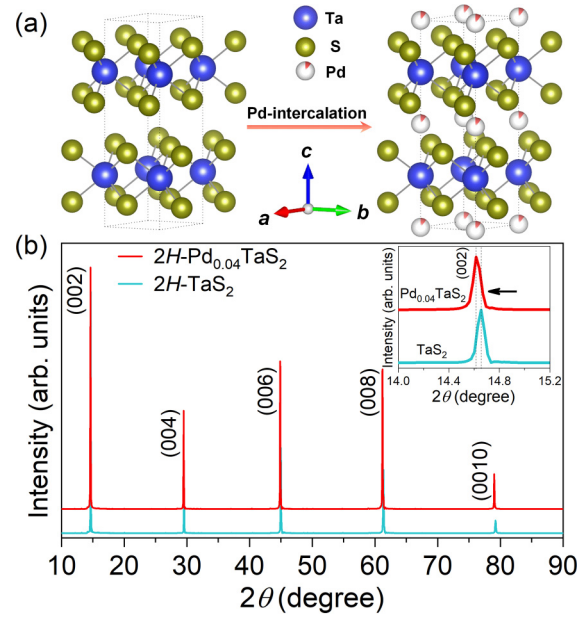

FIG. 1. (a) Crystal structures of pristine and Pd-intercalated $2H$-TaS_2. The two-tone balls represent the disordered distribution of Pd. (b) Pristine and Pd-intercalated $2H$-TaS_2 single-crystal samples exhibit a single preferred ($00l$) orientation, as characterized by x-ray diffraction (XRD) θ-2θ scan. The inset reveals the shift of (002) reflection after Pd intercalation.

layers rather than substitute the intralayer Ta sites. Moreover, such low Pd doping level is generally believed not to induce a change in crystallographic symmetry, i.e., both crystals crystallize in the space group $P6_3/mmc$, which implies that the guest species is disorderedly distributed in the interlayer octahedral interstices of the host as supposed in many metal-intercalated TMDs [51–54], which is schematically illustrated in Fig. 1(a).

The superconducting critical temperature $T_c \sim 0.8$ K for $2H$-TaS_2 was confirmed by the onset of the diamagnetic transition, as shown in Fig. 2(a), in good agreement with the previously reported T_c [55], which reveals that our sample has no stacking faults, Ta self-intercalation, and other imperfections that could cause higher T_c values ranging from 2 to 3.5 K with bulk SC absent [42,50,56]. Upon Pd intercalation, T_c has been enhanced by ~5.6 times, up to 4.5 K in $2H$-$Pd_{0.04}TaS_2$, characterized by magnetic susceptibility and electrical resistivity measurements, as shown in Fig. 2. The T_c value is slightly higher than that reported for polycrystalline $Pd_{0.04}TaS_2$ ($T_c = 4.2$ K) due to the presence of inhomogeneity in the polycrystalline sample [46]. Intriguingly, the T_c of 4.5 K is the highest in the fifth- and sixth-row-metal-intercalated $2H$-TaS_2 reported. The reason for this remains an open question and is pending clarification in the future. Sharp superconducting transition and 100% diamagnetic shielding signal of $2H$-$Pd_{0.04}TaS_2$ single crystal demonstrate the high quality and bulk SC of the sample.

In pristine $2H$-TaS_2, the clearly visible kink on the resistivity $\rho_{ab}(T)$ curve and singular point on the $d\rho_{ab}(T)/dT$ curve in the upper panel of Fig. 3(a) are associated with the emergence of a long-range incommensurate CDW (ICDW)

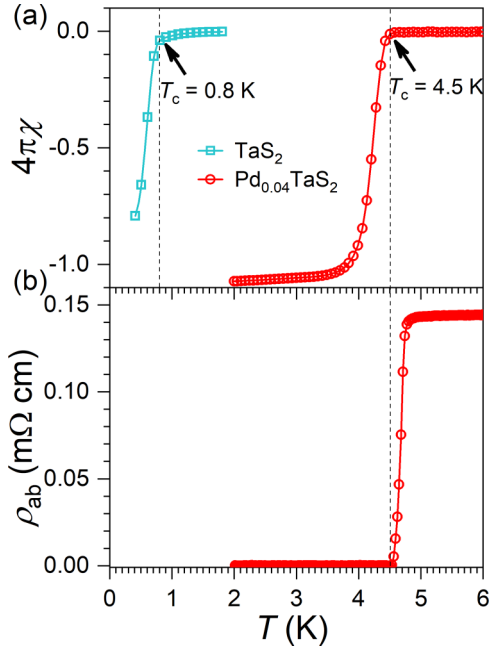

FIG. 2. (a) Temperature dependences of magnetic susceptibility near the superconducting transitions for $2H$-TaS_2 (the square symbols) and $2H$-$Pd_{0.04}TaS_2$ (the circle symbols) single-crystal samples. The data were measured in zero-field-cooling mode and corrected for demagnetization factor. (b) Temperature-dependent in-plane resistivity at low temperature for Pd-intercalated $2H$-TaS_2 single crystal.

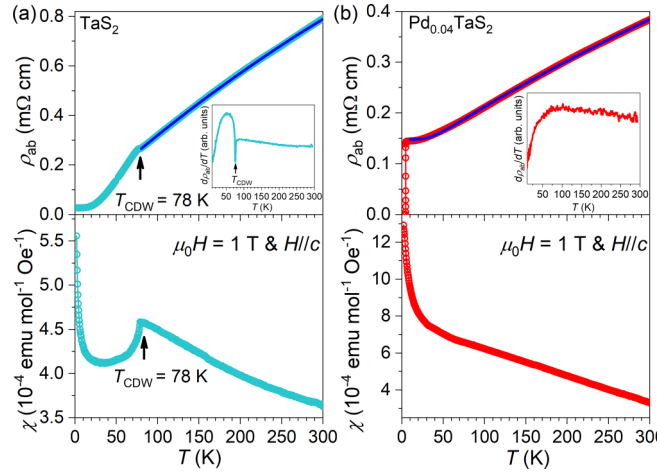

FIG. 3. (a) and (b) The in-plane electrical resistivity (upper panel) and static magnetic susceptibility (lower panel) up to 300 K of $2H$-TaS_2 and $2H$-$Pd_{0.04}TaS_2$ single crystals, the blue solid lines show the fitting of the normal state data by the Bloch-Grüneisen-Mott (BGM) formula. Magnetization is measured under magnetic field $\mu_0 H = 1$ T along the c axis. The insets in (a) and (b) show temperature derivative of in-plane resistivity.

order with $T_{CDW} \sim 78$ K, which is also identified by a significant anomaly on the magnetic susceptibility curve [the lower panel of Fig. 3(a)]. However, such an anomaly is not observed on the resistivity and magnetic susceptibility curves in Fig. 3(b) for $2H$-$Pd_{0.04}TaS_2$, which suggests the absence of CDW transition. Here, T-dependent resistivity above T_{CDW} for $2H$-TaS_2 and above T_c for $Pd_{0.04}TaS_2$ can be well described by the Bloch-Grüneisen-Mott (BGM) formula [57]:

$$\rho(T) = \rho_0 - \alpha T^3 + 4A\left(\frac{T}{\Theta_D^R}\right)^5 \int_0^{\Theta_D^R/T} \frac{x^5}{(e^x - 1)(1 - e^{-x})} dx,$$

where ρ_0 is the T-independent residual resistivity, the second term describes a contribution from the s-d interband scattering, and α is the Mott coefficient. The third term represents a T-dependent resistivity caused by electron-phonon interaction. Here, A is a coupling constant, and Θ_D^R is the Debye temperature. The residual resistivity ratio (RRR $= R_{300K}/R_{78K}$) is reduced from ~3 in TaS_2 to ~2 in $Pd_{0.04}TaS_2$, which again reflects that Pd as scattering centers is successfully introduced into the TaS_2 matrix. Here, A is related to the strength of EPC. The A values are obtained from the fitting as 0.57 and 0.19 mΩ cm for $2H$-TaS_2 and $2H$-$Pd_{0.04}TaS_2$, respectively, which phenomenologically points out that electron-phonon interaction may play an important role in the formation of CDW in this system [36,38,39,58].

Below T_{CDW}, the resistivity $\rho_{ab}(T)$ of the pristine $2H$-TaS_2 drops more rapidly, suggesting an enhanced metallic behavior in the CDW state, but the drop in the susceptibility around T_{CDW} is ascribed to the decrease of the density of states (DOS) at the Fermi level, which is consistent with the opening of the CDW gap. This phenomenological conflict between enhanced metallicity and reduced DOS in the CDW state implies different underlying band structures that govern the two phenomena. This scenario is supported by previous angle-resolved photoemission spectroscopy and optical spectroscopy experiments [58,59], in which the CDW order was found to gap out the Fermi surface around the K point, but leaves the hole pocket Fermi surface around the Γ point unaffected. Thus, it is rational to associate the resistivity behavior with the Γ band and susceptibility with the K band. The absence of any anomaly on the normal-state susceptibility and electrical resistivity of $Pd_{0.04}TaS_2$ evidences the collapse of the long-range ICDW order. The concurrence of the CDW breakdown and the significant SC improvement indicates competition between SC and CDW in the Pd-intercalated $2H$-TaS_2. We notice this competition also observed in other TMDs [3,41,60].

To gain more insight into the evolution of the electronic properties due to Pd intercalation, we performed Hall resistivity measurements on the pristine and Pd-intercalated $2H$-TaS_2 single crystals by sweeping the fields up to 9 T at various fixed temperatures. The Hall resistivity $\rho_{xy}(\mu_0 H)$ of $2H$-TaS_2 is linearly proportional to the magnetic field $\mu_0 H$ above T_{CDW}, while it slightly departs from linearity at the low-field regime below T_{CDW} [Fig. 4(a)], where the transport properties could be understood by a multiband scenario. However, $\rho_{xy}(\mu_0 H)$ of $2H$-$Pd_{0.04}TaS_2$ shows linear behavior with positive slope at all measuring temperatures [Fig. 4(b)]. The Hall coefficient R_H is defined as the magnetic field derivative of $\rho_{xy}(\mu_0 H)$, $R_H = d\rho_{xy}(\mu_0 H)/d(\mu_0 H)$ at the zero-field limit, and the temperature dependences of Hall coefficient $R_H(T)$ are summarized in Fig. 4(c). The Hall coefficient R_H of pristine $2H$-TaS_2 is positive and weakly T dependent above T_{CDW}, decreases rapidly below T_{CDW}, and then changes its sign. The decrease in the R_H below T_{CDW} evidences the weakening of the

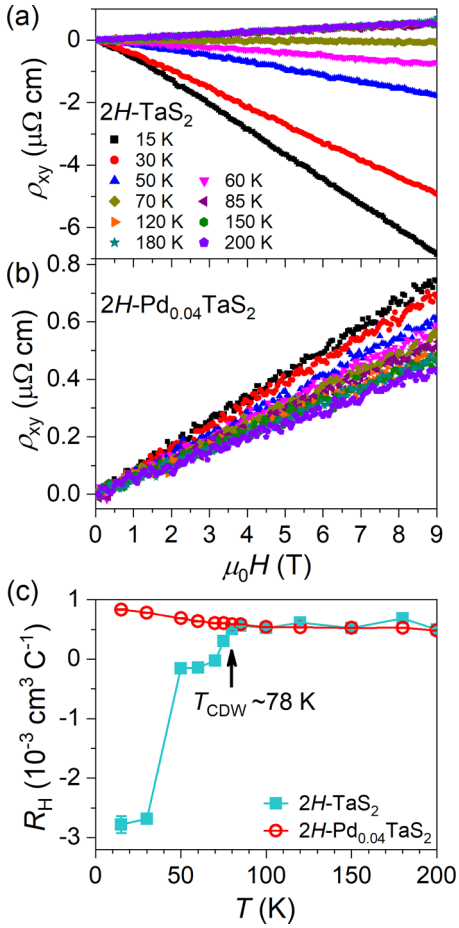

FIG. 4. (a) and (b) Magnetic field dependences of Hall resistivity $\rho_{xy}(\mu_0 H)$ at different temperatures for $2H$-TaS_2 and $2H$-$Pd_{0.04}TaS_2$ single crystals. Not all data are shown for clarity. (c) Temperature dependences of Hall coefficient R_H for $2H$-TaS_2 (the solid square symbols) and $2H$-$Pd_{0.04}TaS_2$ (the hollow circle symbols) single crystals, showing the sign change around $T_{CDW} \sim 78$ K.

contribution from the hole components, which is because the Fermi surface is partially gapped in the CDW state [59]. The positive R_H over the whole temperature range for $Pd_{0.04}TaS_2$ without CDW transition indicates that the hole-type carriers dominate the charge transport in this compound. The temperature dependence is weak, though a gradual increase is observed below 100 K, which implies the possible multiband feature. Such behavior is also observed in $2H$-$Cu_{0.03}TaS_2$ [61] and CDW-free material $2H-NbS_2$ [62]. Almost the same R_H in pristine and intercalated TaS_2 above 78 K suggests comparable carrier concentration in the two cases and negligibly small charge transfer between the intercalant Pd and the parent TaS_2. The rigid band model for layered TMDs, which supposes that minor doping just leads to tiny shift of the Fermi level but could not remarkably modify the band structures [63–66], is inadequate to interpret the striking changes of T_c and transport properties induced by slight Pd intercalating into $2H$-TaS_2. The difference of R_H below 78 K between TaS_2 and $Pd_{0.04}TaS_2$ is attributed to the reconstruction of the Fermi surface by Pd-intercalation-driven collapse of the CDW order. As revealed in Fig. 1(b), Pd intercalation enlarges the van der Waals gap between the TaS_2 layers and could effectively decouple individual layers. This will reduce the interlayer coupling, which could cause the CDW breakdown and SC enhancement, like the effect of thickness reduction [67,68]. In addition, impurity scattering from the disorderly distributed Pd also could disrupt the ordering of the CDW state. Therefore, we believe that the great enhancement of T_c in $2H$-$Pd_{0.04}TaS_2$ is mainly caused by the change of the Fermi surface due to the suppression of CDW instability rather than carrier injection by Pd intercalation.

Further, the increase of carrier concentration with Pd doping was demonstrated by the larger magnetic susceptibility $\chi(T)$ in $2H$-$Pd_{0.04}TaS_2$ than $2H$-TaS_2. Here, $\chi(T)$ of $2H$-$Pd_{0.04}TaS_2$ shows a Curie-Weiss-like behavior at low temperatures possibly owing to a small local moment that stems from the nonmagnetic dopant Pd intercalation, while the difference of carrier concentration at 100 K was estimated only as ~4% according to the formula $n = 1/(eR_H)$. These results indicate tiny charge transfer between Pd and the TaS_2 host layer. The carrier densities at 15 K for $2H$-$Pd_{0.04}TaS_2$ and $2H$-TaS_2 are 7.5×10^{21}holes/cm^3 and 2.2×10^{21}electrons/cm^3, respectively. Therefore, the Pd intercalation does not primarily act as a mechanism for carrier injection but most probably leads to the collapse of the CDW order. The latter causes the development of electronic structure, thereby improved SC.

The CDW transition mechanism and the interplay of SC and CDW phases in $2H$-TaS_2 remain controversial. Fermi surface nesting [34,59] and Fermi patch [69] mechanisms have been applied for understanding the origin of the CDW. Recent studies tend to the notion that the CDW transition in $2H$-TaS_2 is not of Peierls-type origin, and Fermi surface nesting is not the only driven force. Rather, this transition is believed to be induced by momentum-dependent EPC [58,70], which is implicitly reflected by the A value in the BGM formula in this paper. Albeit no consensus has been reached, it is undoubted that the formation of CDW is correlated with both EPC and Fermi surface topology, which are also the links connecting SC with CDW. CDW and SC states are competitive on the Fermi surface. The enhanced T_c in the Pd-intercalated TaS_2 is principally due to the reconstruction of the Fermi surface like that predicted for pressurized $2H$-TaS_2 [70], possibly including the modification of its shape or size and the emergence of additional Fermi pockets. Additionally, EPC may play a role in the evolution of CDW and SC in this system, which needs further study.

IV. CONCLUSIONS

In conclusion, the effect of Pd intercalation on SC and CDW and the interplay between the two ordered states in the $2H$-TaS_2 system have been discussed by transport and magnetic measurements on the high-quality $2H$-TaS_2 and $2H$-$Pd_{0.04}TaS_2$ single crystals. The CDW order breaks down entirely, and T_c increases considerably in $2H$-$Pd_{0.04}TaS_2$, which supports a competitive relation between SC and CDW. The enhancement of SC is mostly ascribed to the change of electronic structure after the suppression of the CDW state. Our results present experimental support for illuminating the physical origin of SC and CDW in $2H$-TaS_2.

ACKNOWLEDGMENTS

We would like to thank Dr. Lingyuan Kong, Dr. Jun Luo for helpful discussion, and Dr. Jianping Sun for his help with magnetic measurement down to 0.4 K. This paper was supported by the National Natural Science Foundation of China (Grants No. 12074414 and No. 11774402), the National Key Research and Development Program of China (Grants No. 2018YFA0704200 and No. 2021YFA1401800), the Strategic Priority Research Program of Chinese Academy of Sciences (Grant No. XDB25000000), and the Synergetic Extreme Condition User Facility (SECUF).

[1] S. Manzeli, D. Ovchinnikov, D. Pasquier, O. V. Yazyev, and A. Kis, Nat. Rev. Mater. **2**, 17033 (2017).

[2] X. Cong, X.-L. Liu, M.-L. Lin, and P.-H. Tan, npj 2D Mater. Appl. **4**, 13 (2020).

[3] B. Sipos, A. F. Kusmartseva, A. Akrap, H. Berger, L. Forró, and E. Tutiš, Nat. Mater. **7**, 960 (2008).

[4] Y. D. Wang, W. L. Yao, Z. M. Xin, T. T. Han, Z. G. Wang, L. Chen, C. Cai, Y. Li, and Y. Zhang, Nat. Commun. **11**, 4215 (2020).

[5] K. T. Law and P. A. Lee, Proc. Natl. Acad. Sci. USA **114**, 6996 (2017).

[6] M. Klanjšek, A. Zorko, R. Žitko, J. Mravlje, Z. Jagličić, P. K. Biswas, P. Prelovšek, D. Mihailovic, and D. Arčon, Nat. Phys. **13**, 1130 (2017).

[7] S. C. de la Barrera, M. R. Sinko, D. P. Gopalan, N. Sivadas, K. L. Seyler, K. Watanabe, T. Taniguchi, A. W. Tsen, X. Xu, D. Xiao *et al.*, Nat. Commun. **9**, 1427 (2018).

[8] J. J. Gao, J. G. Si, X. Luo, J. Yan, Z. Z. Jiang, W. Wang, Y. Y. Han, P. Tong, W. H. Song, X. B. Zhu *et al.*, Phys. Rev. B **102**, 075138 (2020).

[9] A. Ribak, R. M. Skiff, M. Mograbi, P. K. Rout, M. H. Fischer, J. Ruhman, K. Chashka, Y. Dagan, and A. Kanigel, Sci. Adv. **6**, eaax9480 (2020).

[10] I. Guillamón, H. Suderow, J. G. Rodrigo, S. Vieira, P. Rodière, L. Cario, E. Navarro-Moratalla, C. Martí-Gastaldo, and E. Coronado, New J. Phys. **13**, 103020 (2011).

[11] T. Ritschel, J. Trinckauf, G. Garbarino, M. Hanfland, M. v. Zimmermann, H. Berger, B. Büchner, and J. Geck, Phys. Rev. B **87**, 125135 (2013).

[12] D. C. Freitas, P. Rodière, M. R. Osorio, E. Navarro-Moratalla, N. M. Nemes, V. G. Tissen, L. Cario, E. Coronado, M. García-Hernández, S. Vieira *et al.*, Phys. Rev. B **93**, 184512 (2016).

[13] B. Wang, Y. Liu, X. Luo, K. Ishigaki, K. Matsubayashi, W. Lu, Y. Sun, J. Cheng, and Y. Uwatoko, Phys. Rev. B **97**, 220504(R) (2018).

[14] R. Grasset, Y. Gallais, A. Sacuto, M. Cazayous, S. Mañas-Valero, E. Coronado, and M.-A. Méasson, Phys. Rev. Lett. **122**, 127001 (2019).

[15] S. Xu, J. Gao, Z. Liu, K. Chen, P. Yang, S. Tian, C. Gong, J. Sun, M. Xue, J. Gouchi *et al.*, Phys. Rev. B **103**, 224509 (2021).

[16] X. Xi, H. Berger, L. Forró, J. Shan, and K. F. Mak, Phys. Rev. Lett. **117**, 106801 (2016).

[17] M. Yoshida, J. Ye, Y. Zhang, Y. Imai, S. Kimura, A. Fujiwara, T. Nishizaki, N. Kobayashi, M. Nakano, and Y. Iwasa, Nano Lett. **17**, 5567 (2017).

[18] Y. Cui, Z. Hu, J.-S. Zhang, W.-L. Ma, M.-W. Ma, Z. Ma, C. Wang, J.-Q. Yan, J.-P. Sun, J.-G. Cheng *et al.*, Chin. Phys. Lett. **36**, 077401 (2019).

[19] Y. Wu, H. Xing, C.-S. Lian, H. Lian, J. He, W. Duan, J. Liu, Z. Mao, and Y. Liu, Phys. Rev. Mater. **3**, 104003 (2019).

[20] G. Zheng, M. Wang, X. Zhu, C. Tan, J. Wang, S. Albarakati, N. Aloufi, M. Algarni, L. Farrar, M. Wu *et al.*, Nat. Commun. **12**, 3639 (2021).

[21] R. Ang, Y. Tanaka, E. Ieki, K. Nakayama, T. Sato, L. J. Li, W. J. Lu, Y. P. Sun, and T. Takahashi, Phys. Rev. Lett. **109**, 176403 (2012).

[22] L. J. Li, W. J. Lu, X. D. Zhu, L. S. Ling, Z. Qu, and Y. P. Sun, Europhys. Lett. **97**, 67005 (2012).

[23] Y. Liu, R. Ang, W. J. Lu, W. H. Song, L. J. Li, and Y. P. Sun, Appl. Phys. Lett. **102**, 192602 (2013).

[24] R. A. Klemm, Physica C **514**, 86 (2015).

[25] H. Luo, W. Xie, J. Tao, H. Inoue, A. Gyenis, J. W. Krizan, A. Yazdani, Y. Zhu, and R. J. Cava, Proc. Natl. Acad. Sci. USA **112**, E1174 (2015).

[26] Y. Liu, D. F. Shao, L. J. Li, W. J. Lu, X. D. Zhu, P. Tong, R. C. Xiao, L. S. Ling, C. Y. Xi, L. Pi *et al.*, Phys. Rev. B **94**, 045131 (2016).

[27] L. Li, X. Deng, Z. Wang, Y. Liu, M. Abeykoon, E. Dooryhee, A. Tomic, Y. Huang, J. B. Warren, E. S. Bozin *et al.*, npj Quant. Mater. **2**, 11 (2017).

[28] H. Bai, M. Wang, X. Yang, Y. Li, J. Ma, X. Sun, Q. Tao, L. Li, and Z.-A. Xu, J. Phys.: Condens. Matter **30**, 095703 (2018).

[29] J. J. Gao, W. H. Zhang, J. G. Si, X. Luo, J. Yan, Z. Z. Jiang, W. Wang, H. Y. Lv, P. Tong, W. H. Song *et al.*, Appl. Phys. Lett. **118**, 213105 (2021).

[30] Y. Liu, L. J. Li, W. J. Lu, R. Ang, X. Z. Liu, and Y. P. Sun, J. Appl. Phys. **115**, 043915 (2014).

[31] M. Bazarnik, R. Lo Conte, E. Mascot, K. von Bergmann, D. K. Morr, and R. Wiesendanger, Nat. Commun. **14**, 614 (2023).

[32] V. Vaňo, M. Amini, S. C. Ganguli, G. Chen, J. L. Lado, S. Kezilebieke, and P. Liljeroth, Nature (London) **599**, 582 (2021).

[33] E. Persky, A. V. Bjørlig, I. Feldman, A. Almoalem, E. Altman, E. Berg, I. Kimchi, J. Ruhman, A. Kanigel, and B. Kalisky, Nature (London) **607**, 692 (2022).

[34] J. A. Wilson, Phys. Rev. B **15**, 5748 (1977).

[35] T. M. Rice and G. K. Scott, Phys. Rev. Lett. **35**, 120 (1975).

[36] C. M. Varma and A. L. Simons, Phys. Rev. Lett. **51**, 138 (1983).

[37] L. P. Gor'kov, Phys. Rev. B **85**, 165142 (2012).

[38] F. Flicker and J. van Wezel, Nat. Commun. **6**, 7034 (2015).

[39] F. Flicker and J. van Wezel, Phys. Rev. B **94**, 235135 (2016).

[40] Y. Kashihara, A. Nishida, and H. Yoshioka, J. Phys. Soc. Jpn. **46**, 1112 (1979).

[41] L. Fang, Y. Wang, P. Y. Zou, L. Tang, Z. Xu, H. Chen, C. Dong, L. Shan, and H. H. Wen, Phys. Rev. B **72**, 014534 (2005).

[42] K. E. Wagner, E. Morosan, Y. S. Hor, J. Tao, Y. Zhu, T. Sanders, T. M. McQueen, H. W. Zandbergen, A. J. Williams, D. V. West *et al.*, Phys. Rev. B **78**, 104520 (2008).

[43] L. J. Li, X. D. Zhu, Y. P. Sun, H. C. Lei, B. S. Wang, S. B. Zhang, X. B. Zhu, Z. R. Yang, and W. H. Song, Physica C **470**, 313 (2010).
[44] N. Z. Wang, M. Z. Shi, C. Shang, F. B. Meng, L. K. Ma, X. G. Luo, and X. H. Chen, New J. Phys. **20**, 023014 (2018).
[45] H. Liu, S. Huangfu, X. Zhang, H. Lin, and A. Schilling, Phys. Rev. B **104**, 064511 (2021).
[46] M. H. Zhou, X. C. Li, and C. Dong, Supercond. Sci. Technol. **31**, 065001 (2018).
[47] J. Zhou, J. Lin, X. Huang, Y. Zhou, Y. Chen, J. Xia, H. Wang, Y. Xie, H. Yu, J. Lei *et al.*, Nature (London) **556**, 355 (2018).
[48] K. Hayashi, T. Ikeuchi, H. Takeuchi, and M. Shimakawa, J. Alloys Compounds **219**, 161 (1995).
[49] X. C. Li, M. H. Zhou, and C. Dong, Supercond. Sci. Technol. **32**, 035001 (2019).
[50] S. Nagata, T. Aochi, T. Abe, S. Ebisu, T. Hagino, Y. Seki, and K. Tsutsumi, J. Phys. Chem. Solids **53**, 1259 (1992).
[51] J. M. Voorhoeve, N. van den Berg, and M. Robbins, J. Solid State Chem. **1**, 134 (1970).
[52] F. J. Di Salvo, G. W. Hull, Jr., L. H. Schwartz, J. M. Voorhoeve, and J. V. Waszczak, J. Chem. Phys. **59**, 1922 (1973).
[53] M. Kars, A. Gómez-Herrero, A. Rebbah, and L. C. Otero-Diáz, Mater. Res. Bull. **44**, 1601 (2009).
[54] X. C. Li, M. H. Zhou, L. H. Yang, and C. Dong, Supercond. Sci. Technol. **30**, 125001 (2017).
[55] J. M. E. Harper, T. H. Geballe, and F. J. DiSalvo, Phys. Rev. B **15**, 2943 (1977).
[56] L. J. Li, W. J. Lu, Y. Liu, Z. Qu, L. S. Ling, and Y. P. Sun, Physica C **492**, 64 (2013).
[57] N. F. Mott, Adv. Phys. **13**, 325 (1964).
[58] K. Wijayaratne, J. Zhao, C. Malliakas, D. Y. Chung, M. G. Kanatzidis, and U. Chatterjee, J. Mater. Chem. C **5**, 11310 (2017).
[59] W. Z. Hu, G. Li, J. Yan, H. H. Wen, G. Wu, X. H. Chen, and N. L. Wang, Phys. Rev. B **76**, 045103 (2007).
[60] E. Morosan, H. W. Zandbergen, B. S. Dennis, J. W. G. Bos, Y. Onose, T. Klimczuk, A. P. Ramirez, N. P. Ong, and R. J. Cava, Nat. Phys. **2**, 544 (2006).
[61] X. D. Zhu, Y. P. Sun, X. B. Zhu, X. Luo, B. S. Wang, G. Li, Z. R. Yang, W. H. Song, and J. M. Dai, J. Cryst. Growth **311**, 218 (2008).
[62] M. Naito and S. Tanaka, J. Phys. Soc. Jpn. **51**, 219 (1982).
[63] G. Y. Guo and W. Y. Liang, J. Phys. C: Solid State Phys. **20**, 4315 (1987).
[64] P. Blaha, J. Phys.: Condens. Matter **3**, 9381 (1991).
[65] K. Motizuki, N. Suzuki, and S. Tomishima, J. Magn. Magn. Mater. **104–107**, 681 (1992).
[66] H. P. Hughes and J. A. Scarfe, J. Phys.: Condens. Matter **8**, 1439 (1996).
[67] Y. Yang, S. Fang, V. Fatemi, J. Ruhman, E. Navarro-Moratalla, K. Watanabe, T. Taniguchi, E. Kaxiras, and P. Jarillo-Herrero, Phys. Rev. B **98**, 035203 (2018).
[68] D. Lin, S. Li, J. Wen, H. Berger, L. Forró, H. Zhou, S. Jia, T. Taniguchi, K. Watanabe, X. Xi *et al.*, Nat. Commun. **11**, 2406 (2020).
[69] D. W. Shen, B. P. Xie, J. F. Zhao, L. X. Yang, L. Fang, J. Shi, R. H. He, D. H. Lu, H. H. Wen, and D. L. Feng, Phys. Rev. Lett. **99**, 216404 (2007).
[70] Y. Kvashnin, D. VanGennep, M. Mito, S. A. Medvedev, R. Thiyagarajan, O. Karis, A. N. Vasiliev, O. Eriksson, and M. Abdel-Hafiez, Phys. Rev. Lett. **125**, 186401 (2020).